Available online at www.sciencedirect.com
ScienceDirect
Trans. Nonferrous Met. Soc. China 31(2021) 1766−1783
Transactions of Nonferrous Metals Society of China
www.tnmsc.cn

Analyses and predictions of rock cuttabilities under different confining stresses and rock properties based on rock indentation tests by conical pick

Shao-feng WANG[1], Yu TANG[1], Xi-bing LI[1], Kun DU[1,2]

1. School of Resources and Safety Engineering, Central South University, Changsha 410083, China;
2. Advanced Research Center, Central South University, Changsha 410083, China

Received 10 July 2020; accepted 24 December 2020

Abstract: The rock indentation tests by a conical pick were conducted to investigate the rock cuttability correlated to confining stress conditions and rock strength. Based on the test results, the regression analyses, support vector machine (SVM) and generalized regression neural network (GRNN) were used to find the relationship among rock cuttability, uniaxial confining stress applied to rock, uniaxial compressive strength (UCS) and tensile strength of rock material. It was found that the regression and SVM-based models can accurately reflect the variation law of rock cuttability, which presented decreases followed by increases with the increase in uniaxial confining stress and the negative correlation to UCS and tensile strength of rock material. Based on prediction models for revealing the optimal stress condition and determining the cutting parameters, the axial boom roadheader with many conical picks mounted was satisfactorily utilized to perform rock cutting in hard phosphate rock around pillar.

Key words: rock cuttability; rock indentation; prediction model; regression analysis; support vector machine; neural network

1 Introduction

Mechanized excavation is a widely used method in rock engineering, which can be as an alternative approach to drilling and blasting method, resulting from its numerous advantages: continuous and safe operation, high quality of construction and low excavation disturbance [1−3]. Rock cuttability is a comprehensive parameter reflecting the interaction between cutter and rock, which determines the feasibility of mechanized excavation. Rock cuttability is influenced by rock properties and stress conditions [4]. Mechanized excavation method has been widely used in soft and medium-hard rock, such as coal, bauxite and salt minerals, while it is unsuitable for extremely hard rock. The high stress and high temperature at interaction between rock and cutter will cause serious pick wear failures and high mining costs during hard rock cutting [5]. However, it is worth noting that deep mining of non-ferrous metals at depths greater than 1 km is often in hard rock mines [6]. Therefore, the application of mechanized excavation in hard rock is an urgent problem and should be addressed in deep mining. High stress is a prominent condition in hardrock around deep opening, which had been traditionally considered as a disaster factor to induce instability and dynamic failure of rock, such as rockburst, large deformation, slabbing and zonal disintegration [7−12].

Many previous efforts had been taken to study the rock cuttability. In experimental investigations, the multiform approaches had been undertaken,

Corresponding author: Kun DU, E-mail: dukuncsu@csu.edu.cn
DOI: 10.1016/S1003-6326(21)65615-7

which included full-scale and small-scale cutting experiments, linear and rotary cutting tests, single- and multi-cutter cutting tests, and so on. These experiments were taken to study the cutting force, cutting work, specific energy, fragment yield, shape and size of fragments, fractured surface roughness and wear of cutter under different conditions of rock properties and cutting operations [13−15]. In terms of theoretical models, some analytical and semi-empirical expressions have been proposed to determine the peak cutting force of conical cutter [16,17]. For numerical simulations, the finite element method (FEM), discrete element method (DEM) and coupled FEM−DEM method have been used to simulate the rock fragmentation by conical or point-attack cutters to trace the complex fracturing process and reduce the costs [18,19]. In addition, artificial intelligence (AI)-based approaches, such as artificial neural network (ANN), adaptive neuro fuzzy inference system (ANFIS), fuzzy logic, particle swarm optimization (PSO) and support vector machine (SVM), have been used to estimate the parameters of tunnel boring machine (TBM) performances including advance rate (AR) and penetration rate (PR) [20−26]. The valuable studies mentioned above play a significant role in understanding rock cuttabilities and cutting performances under different rock properties and cutting parameters. However, the previous efforts did not consider the influence of confining stress condition that can be ignored in shallow excavations but is a common factor in deep mining and tunneling [27].

In this work, the rock indentation tests by a conical pick under different uniaxial confining stress conditions were conducted on the granite, marble, red sandstone and phosphate rocks by using the true-triaxial loading system. The peak indentation force, peak indentation depth, cutting work and specific energy of conical pick for rock breakage were used to determine the rock cuttability. Then, the two- and three-dimensional regression analyses and AI-based approaches including SVM and generalized regression neural network (GRNN) were used to establish the models of rock cuttability correlated with the confining stress conditions and rock strength properties. Finally, the transverse roadheader having many conical picks was utilized to perform field cutting in rock around pillar.

2 Rock indentation experiments

2.1 Experimental apparatus

The rock indentation experiments were performed with TRW−3000 true triaxial electro-hydraulic servo test system shown in Fig. 1, which was designed and manufactured by Central South University, China. This system can perform rock loading tests under triaxial, biaxial, uniaxial stress conditions. The maximum static loads in the *X*-, *Y*- and *Z*-direction can reach 2000, 2000 and 3000 kN, respectively.

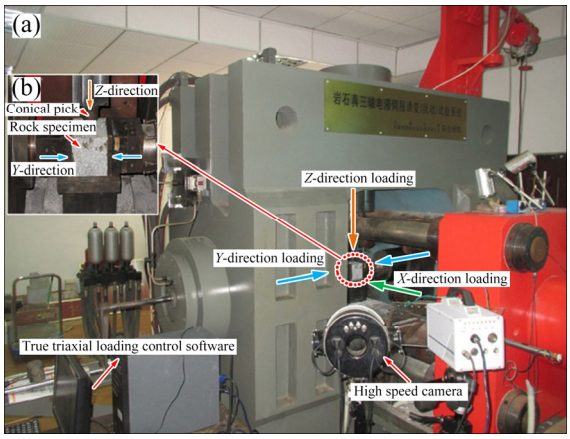

Fig. 1 TRW−3000 true triaxial electro-hydraulic servo system for true triaxial loading test: (a) True triaxial loading system; (b) Loading frame of rock indentation by conical pick

2.2 Rock specimens

The granite, marble, red sandstone and phosphate rock specimens were selected in rock indentation experiments, which were all cubic rock specimens with size of 100 mm × 100 mm × 100 mm. There were 35 groups of rock specimens, including 9 groups of granites, 9 groups of marbles, 8 groups of red sandstones, and 9 groups of phosphate rocks. The uniaxial compressive strength (UCS) and tensile strength of rock materials are listed in Table 1.

2.3 Experimental processes

In order to simulate the rock breakage on pillar by conical picks mounted on the mining machine such as roadheader, the rock indentation tests were conducted on cubic rock specimens, which were subjected to uniaxial confining stress on a pair of

lateral end faces and broken by a conical pick, as shown in Fig. 2. The loading frame is shown in Fig. 2(b). Firstly, the uniaxial confining stress was applied to the left and right lateral end faces of rock specimen by *Y*-direction loading. Then, a concentrated force was applied to a conical pick by *Z*-direction loading until rock breakage.

Table 1 Strengths of rock materials used in tests

Rock type	Uniaxial compressive strength, σ_c/MPa	Tensile strength, σ_t/MPa
Granite	126.24	7.56
Marble	129.22	6.18
Red sandstone	97.79	5.31
Phosphate rock	106.21	5.24

In the rock indentation tests, the nine groups of granite rock specimens and the nine groups of marble rock specimen were tested under uniaxial confining stresses of 5, 10, 20, 40, 60, 80, 100, 120 MPa and stress-free condition (0 MPa), respectively. The eight groups of red sandstone rock specimens were tested under uniaxial confining stress of 5, 10, 20, 40, 60, 80, 90 MPa and stress-free condition (0 MPa), respectively. The nine groups of phosphate rock specimens were tested under uniaxial confining stress of 5, 10, 20, 40, 60, 80, 90, 100 MPa and stress-free condition (0 MPa), respectively.

The indentation forces and depths of conical pick can be directly fed back to the computer through the load and displacement monitoring sensors during tests. The peak indentation force and depth at rock failure can be extracted from the real-time monitoring data of the indentation force and depth of conical pick. The cutting work can be calculated by Eq. (1). Meanwhile, the volume of rock fragments broken from rock specimen can be measured after the experiment, and then the specific energy can be calculated by Eq. (2). The rock cuttability can be reflected by peak indentation force, peak indentation depth, cutting work and specific energy for rock breakage, and the low values of these indices indicate the good rock cuttability. Among these parameters, the peak indentation force and specific energy are key factors to determine the cuttability of rock, which represent the load and energy required for cutting rock.

$$W_c = 1/2 F_c D_c \tag{1}$$

$$E_c = W_c / V_c \tag{2}$$

where W_c and E_c are the tested cutting work and specific energy for rock breakage, respectively; F_c and D_c are the peak indentation force and depth at rock failure measured in the rock indentation tests, respectively; V_c is the volume of fragments cut by the conical pick under different uniaxial confining stresses.

2.4 Experimental results

According to experimental results and the associated calculations, the results of peak indentation force, peak indentation depth, cutting work, specific energy of granite, marble, red sandstone, and phosphate rocks under different uniaxial confining stress conditions are given in Table 2.

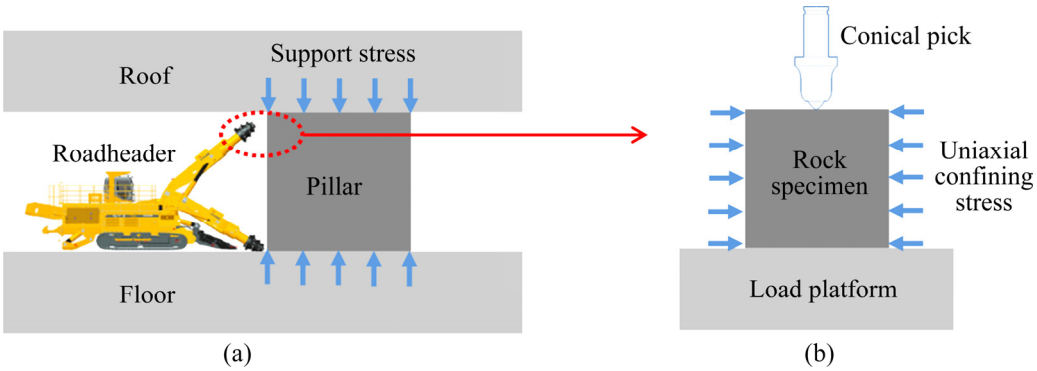

Fig. 2 Loading condition for simulating rock indentation on pillar by conical pick: (a) Schematic mining process for cutting pillar; (b) Simplified loading platform

Table 2 Experimental results of rock indentation tests

Rock type	Uniaxial confining pressure, σ_y/MPa	Peak indentation force, F_c/kN	Peak indentation depth, D_c/mm	Cutting work, W_c/J	Specific energy, E_c/(10^{-3}J·cm^{-3})
Granite	120	114.27	3.74	213.68	213.68
	100	140.14	5.39	377.68	377.68
	80	148.95	9.10	677.72	5421.76
	60	162.33	12.19	989.40	7915.20
	40	206.28	12.27	1265.53	5062.12
	20	203.44	11.25	1144.35	3433.08
	10	76.45	5.34	204.12	510.30
	5	63.77	3.43	109.37	240.61
	0	50.03	2.69	67.29	134.58
Marble	120	100.07	5.17	258.68	258.68
	100	138.34	8.04	556.13	556.13
	80	160.83	12.08	971.41	7771.28
	60	188.90	12.83	1211.79	9694.32
	40	217.90	13.04	1420.71	4972.56
	20	183.26	12.07	1105.97	3317.94
	10	62.89	6.03	189.61	474.03
	5	43.42	5.61	121.79	267.94
	0	34.84	5.15	89.71	179.42
Red sandstone	90	25.13	3.24	40.71	40.71
	80	58.71	6.41	188.17	188.17
	60	78.93	7.32	288.88	2311.04
	40	112.15	9.45	529.91	2649.55
	20	103.62	8.64	447.64	1342.93
	10	42.33	5.17	109.42	273.55
	5	31.55	4.13	65.15	143.33
	0	16.24	3.04	24.68	49.36
Phosphate rock	100	23.15	3.61	41.79	41.79
	90	45.21	4.21	95.17	95.17
	80	68.74	6.55	225.12	1800.96
	60	100.92	8.64	435.97	3487.76
	40	142.17	11.23	798.28	2794.02
	20	113.62	9.31	528.90	1586.72
	10	32.33	4.12	66.60	166.50
	5	16.51	3.23	26.66	58.65
	0	5.26	3.01	7.92	15.84

3 Regression analyses

In order to find the relationships between rock cuttabilities and rock properties under different uniaxial confining stress, a series of regression models were established.

3.1 Two-dimensional regression

3.1.1 Granite rock specimens

The four models were established and regressed by experimental results of granite rock specimens, as expressed in Table 3 to reflect the peak indentation force, peak indentation depth, cutting work and specific energy influenced by

Table 3 Regression models for different rocks

Rock sample	Regression model
Granite	$F_c = 63.36\times(0.01007\sigma_y^2 e^{-0.04806\sigma_y}+1)$
	$D_c = 2.485\times(0.02124\sigma_y^2 e^{-0.05066\sigma_y}+1)$
	$W_c = 7.219\times(0.9478\sigma_y^2 e^{-0.05292\sigma_y}+1)$
	$E_c = 15.09\times(0.004216\sigma_y^4 e^{-0.07998\sigma_y}+1)$
Marble	$F_c = 39.94\times(0.01663\sigma_y^2 e^{-0.04411\sigma_y}+1)$
	$D_c = 4.568\times(0.008602\sigma_y^2 e^{-0.04697\sigma_y}+1)$
	$W_c = 4.466\times(1.357\sigma_y^2 e^{-0.04732\sigma_y}+1)$
	$E_c = 0.9786\times(0.05713\sigma_y^4 e^{-0.0747\sigma_y}+1)$
Red sandstone	$F_c = 13.04\times(0.05553\sigma_y^2 e^{-0.06109\sigma_y}+1)$
	$D_c = 2.921\times(0.01612\sigma_y^2 e^{-0.06074\sigma_y}+1)$
	$W_c = 0.2808\times(13.18\sigma_y^2 e^{-0.06241\sigma_y}+1)$
	$E_c = 0.07381\times(0.9544\sigma_y^4 e^{-0.1042\sigma_y}+1)$
Phosphate rock	$F_c = 0.1086\times(7.456\sigma_y^2 e^{-0.05547\sigma_y}+1)$
	$D_c = 2.102\times(0.02524\sigma_y^2 e^{-0.05614\sigma_y}+1)$
	$W_c = 0.5119\times(8.564\sigma_y^2 e^{-0.05915\sigma_y}+1)$
	$E_c = 0.05091\times(0.9784\sigma_y^4 e^{-0.09093\sigma_y}+1)$

uniaxial confining stress. The regressive curves are plotted in Figs. 3−6. By analyzing the experimental and regressive results of granite rock specimens and the failure patterns, the variation trend of peak indentation force, peak indentation depth and cutting work can be divided into three zones. In Zone 1 with uniaxial confining stress varying from 0 to 40 MPa (near 30% of UCS of granite material), there was a positive correlation in which the peak indentation force, peak indentation depth and cutting work increased with the increase in uniaxial confining stress, and the failure pattern was complete splitting. In Zone 2 with the uniaxial confining stress varying from 40 to 100 MPa (near 80% of UCS of granite material), there was a negative correlation in which the peak indentation force, peak indentation depth and cutting work decreased with the increase in the uniaxial confining stress, and the failure pattern of rock was partial splitting. In Zone 3 with uniaxial confining stress exceeding 100 MPa, the peak indentation force, peak indentation depth and cutting work continued to decrease, and the rockburst occurred

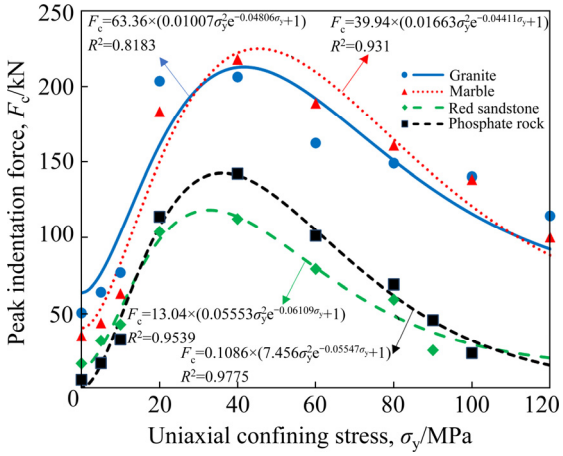

Fig. 3 Regressed curves of peak indentation forces for four types of rock specimens

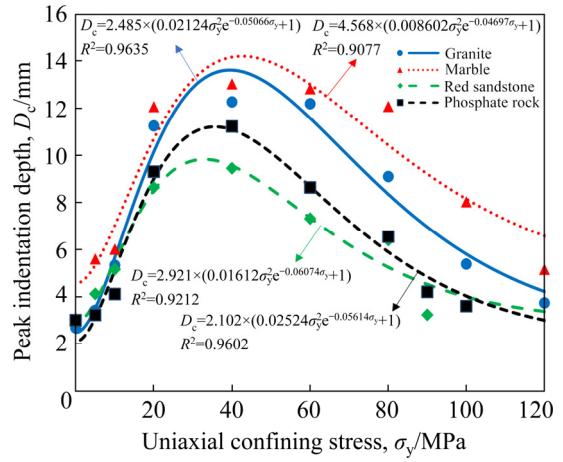

Fig. 4 Regressed curves of peak indentation depths for four types of rock specimens

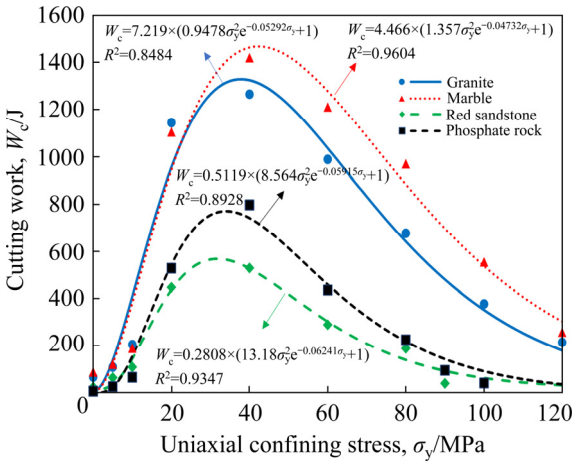

Fig. 5 Regressed curves of cutting work for four types of rock specimens

(In experiment, the failure of rock specimen occurs with a large number of rock fragments ejected at high speed, which is called as experimental rockburst).

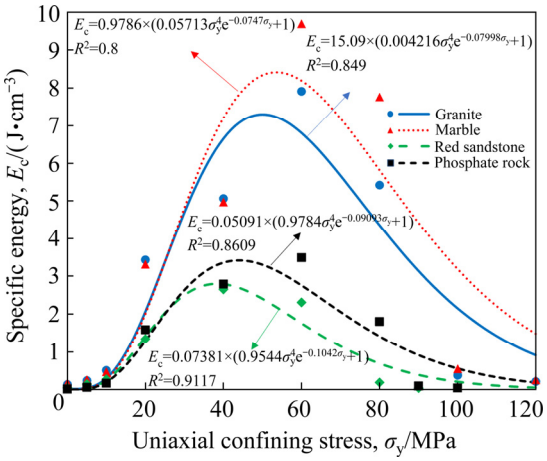

Fig. 6 Regressed curves of specific energy for four types of rock specimens

According to the changing trend of specific energy, there was also three zones. In Zone 1 with uniaxial confining stress increasing from 0 to 60 MPa (near 50% of UCS of granite material), the specific energy increased with the increase in uniaxial confining stress. In Zone 2 with uniaxial confining stress increasing from 60 to 100 MPa (near 80% of UCS of granite material), the specific energy decreased with the increase in uniaxial confining stress. In Zone 3 with uniaxial confining stress increasing beyond 100 MPa, the specific energy decreased to the very low values with the rockburst occurring.

The detailed failure modes of rocks had been shown in our previous work [4].

3.1.2 Marble rock specimens

The variation curves of peak indentation force, peak indentation depth, cutting work and specific energy of conical pick for breakage of marble rock specimens were also regressed by experimental values, as given in Table 3 and shown in Figs. 3−6. There were three zones reflecting the variation characteristic. In Zone 1 with uniaxial confining stress in the range of 0−40 MPa (near 30% of UCS of marble material), the peak indentation force, peak indentation depth and cutting work increased with the increase in uniaxial confining stress, and the failure pattern is complete splitting. In Zone 2 with uniaxial confining stress changing in the range of 40−100 MPa (near 80% of UCS of marble material), the peak indentation force, peak indentation depth and cutting work decreased with the increase in uniaxial confining stress, and the failure pattern was partial splitting. In Zone 3 with uniaxial confining stress exceeding 100 MPa, the peak indentation force, peak indentation depth and cutting work continued to decrease into the very low values, and the failure pattern was rockburst. The specific energy increased first and then decreased with the uniaxial confining stress increasing in the range of 0−60 MPa (near 50% of UCS of marble material) and 60−100 MPa, respectively. In addition, the specific energy continued to decrease and had a very low value when the uniaxial confining stress exceeded 100 MPa.

3.1.3 Red sandstone rock specimens

The peak indentation force, peak indentation depth, cutting work and specific energy of conical pick for breakages of red sandstone rock specimens influenced by uniaxial confining stresses are shown in Table 3 and Figs. 3−6. Similar to the granite and marble, the peak indentation force, peak indentation depth and cutting work increased first and then decreased with the increase in uniaxial confining stress in the range of 0−40 MPa (near 40% of UCS of red sandstone material) and 40−80 MPa (near 80% of UCS of red sandstone material), respectively, and the failure patterns changed from complete splitting to partial splitting. The peak indentation force, peak indentation depth and cutting work continued to decrease with the increase of uniaxial confining stress exceeding 80 MPa, and the failure pattern was rockburst. The specific energy increased first and then decreased with the uniaxial confining stress increasing in the range of 0−40 MPa and 40−80 MPa, respectively. In addition, the specific energy continued to decrease and had a very low value when the uniaxial confining stress exceeded 80 MPa with rockburst occurring.

3.1.4 Phosphate rock specimens

The peak indentation force, peak indentation depth, cutting work and specific energy of conical pick for breakages of phosphate rock specimens influenced by uniaxial confining stresses are shown in Table 3 and Figs. 3−6. Similar to the granite, marble and red sandstone, the peak indentation force, peak indentation depth and cutting work presented increase followed by decrease with the increase in uniaxial confining stress in the ranges of 0−40 MPa (near 40% of UCS of phosphate material) and 40−90 MPa (near 80% of UCS of phosphate material), respectively, and the failure

patterns changed from complete splitting to partial splitting. The peak indentation force, peak indentation depth and cutting work continued to decrease with the increase of uniaxial confining stress exceeding 90 MPa, and the rockburst occurred under this high uniaxial confining stress. The specific energy also presented increase followed by decrease with the uniaxial confining stress increasing in the ranges of 0−60 MPa (near 55% of UCS of phosphate rock) and 60−90 MPa, respectively. In addition, the specific energy continued to decrease and had a very low value when the uniaxial confining stress exceeded 90 MPa, in which the rockburst occurred.

3.1.5 Evaluation of regression models

In order to evaluate the reliabilities of regression models, we evaluated each model using the root-mean-squared error (RMSE) and determination coefficient (R^2) expressed as Eq. (3) and Eq. (4), respectively. The corresponding RMSE and R^2 values were obtained by calculation, as listed in Table 4.

$$\mathrm{RMSE}=\sqrt{\frac{1}{n}\sum_{i=1}^{n}(y_{\mathrm{t}(i)}-y_{\mathrm{p}(i)})^2} \tag{3}$$

$$R^2=\sum_{i=1}^{n}(y_{\mathrm{p}(i)}-\overline{y}_{\mathrm{t}})^2/\sum_{i=1}^{n}(y_{\mathrm{t}(i)}-\overline{y}_{\mathrm{t}})^2 \tag{4}$$

where $y_{\mathrm{t}(i)}$ is the experimental value, $y_{\mathrm{p}(i)}$ is the regression value, $\overline{y}_{\mathrm{t}}$ is the mean of all experimental values, and n is the number of values.

3.2 Three-dimensional regression

In order to characterize the influence of rock properties and uniaxial confining stress conditions on the rock cuttabilities reflected by peak indentation force, peak indentation depth, cutting work and specific energy, three-dimensional regression analyses were taken by the experimental data obtained from rock indentation tests. The UCS and tensile strength of rock material were used to determine rock properties.

3.2.1 Peak indentation forces

The USC values of granite, marble, red sandstone and phosphate rock materials were taken as the X-axis, the different uniaxial confining stresses applied to rock specimens were taken as the Y-axis, and the peak pick forces applied to conical pick for rock breakages were taken as the Z-axis. The curved surface was obtained by three-dimensional regression to express the relationship among peak indentation force, UCS of rock materials and uniaxial confining stress, and the expression and illustration are shown in Eq. (5) and Fig. 7, respectively. The product of UCS and tensile strength was taken as the X-axis, but keep the Y-axis and Z-axis parameters unchanged. Another curved surface was achieved, as shown in Eq. (6) and Fig. 8.

$$F_{\mathrm{c}}=5.904\times(2.854\times10^{-5}\sigma_{\mathrm{c}}^{2.2}\sigma_{\mathrm{y}}^{3}\,\mathrm{e}^{-1.771\sigma_{\mathrm{y}}^{0.4}}+1) \tag{5}$$

$$F_{\mathrm{c}}=28.51\times(7.137\times10^{-8}\sigma_{\mathrm{c}}^{2.2}\sigma_{\mathrm{t}}^{2.2}\sigma_{\mathrm{y}}^{3}\,\mathrm{e}^{-1.758\sigma_{\mathrm{y}}^{0.4}}+1) \tag{6}$$

3.2.2 Peak indentation depth

Similar to the regression analyses of peak indentation force, the curved surfaces of peak indentation depths correlated to UCS, tensile strength of rock material and uniaxial confining stress were regressed by experimental data. The regressed expressions are given in Eqs. (7) and (8), and the curved surfaces are shown in Figs. 9 and 10, respectively.

$$D_{\mathrm{c}}=2.538\times(2.473\times10^{-6}\sigma_{\mathrm{c}}^{2}\sigma_{\mathrm{y}}^{3}\,\mathrm{e}^{-1.009\sigma_{\mathrm{y}}^{0.5}}+1) \tag{7}$$

$$D_{\mathrm{c}}=3.341\times(5.242\times10^{-6}\sigma_{\mathrm{c}}\sigma_{\mathrm{t}}\sigma_{\mathrm{y}}^{3}\,\mathrm{e}^{-0.341\sigma_{\mathrm{y}}^{0.7}}+1) \tag{8}$$

3.2.3 Cutting work

Similarly, the curved surfaces of cutting work influenced by UCS, tensile strength of rock material

Table 4 RMSE and R^2 values of two-dimensional fitting models for different rock types

Rock type	Peak indentation force		Peak indentation depth		Cutting work		Specific energy	
	RMSE/kN	R^2	RMSE/mm	R^2	RMSE/J	R^2	RMSE/(10^{-3}J·cm^{-3})	R^2
Granite	28.390	0.8183	0.8683	0.9635	106.70	0.9484	1324	0.849
Marble	20.580	0.9310	1.2430	0.9077	104.00	0.9604	1887	0.800
Red sandstone	9.216	0.9539	0.8069	0.9212	53.13	0.9347	379.9	0.9117
Phosphate rock	7.235	0.9775	0.7041	0.9602	97.64	0.8928	581.1	0.8609

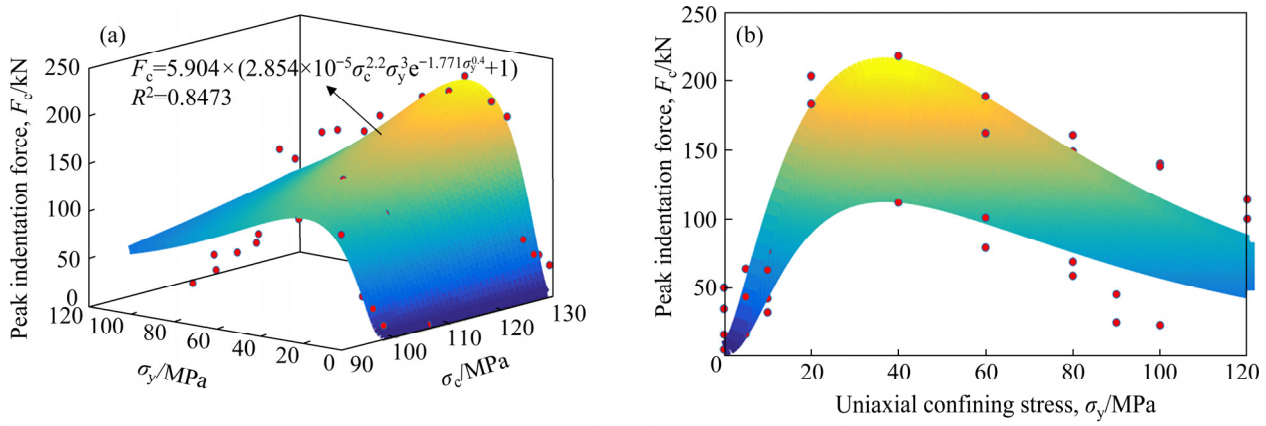

Fig. 7 Regressed curved surface of peak indentation force correlated to UCS of rock material and uniaxial confining stress: (a) Three-dimensional view of curved surface; (b) View of curved surface from *X*-axis

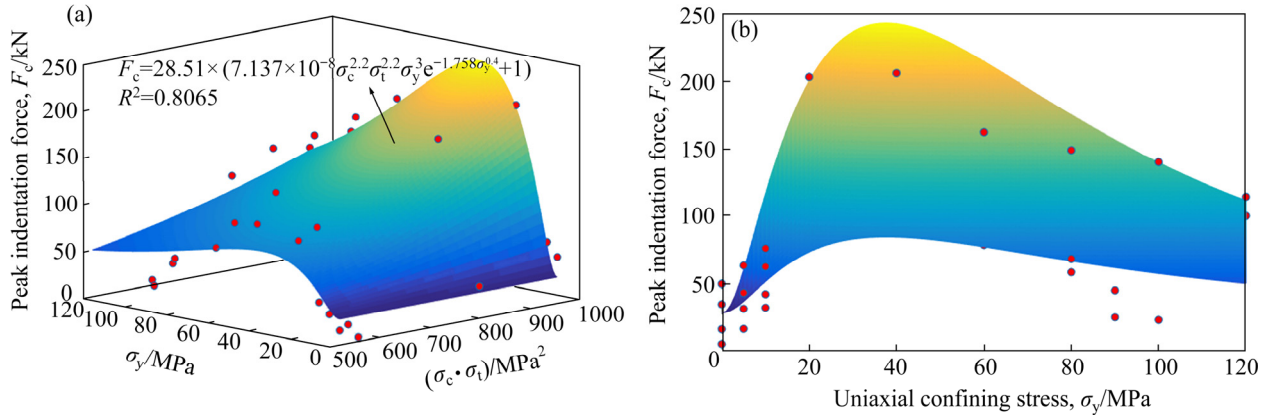

Fig. 8 Regressed curved surface of peak indentation force correlated with uniaxial confining stress and product of UCS and tensile strength: (a) Three-dimensional view of regressed curved surface; (b) View of regressed curved surface from *X*-axis

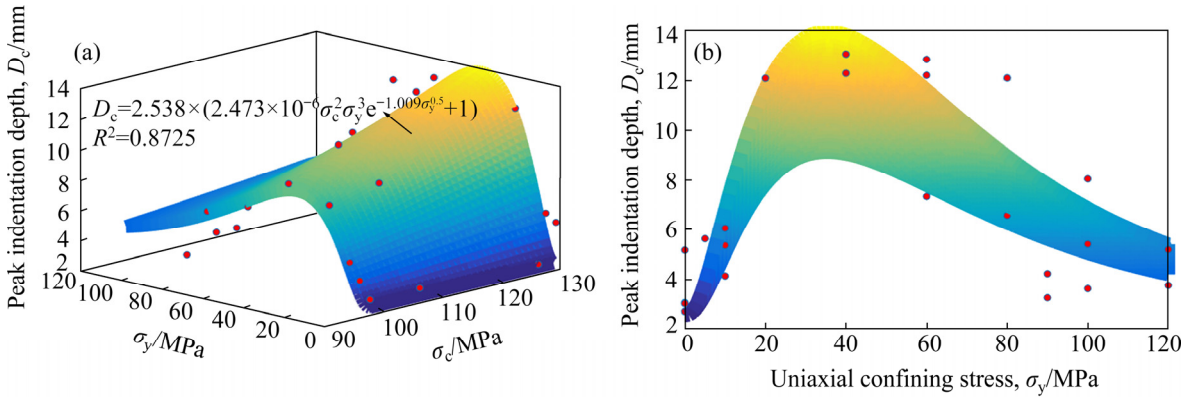

Fig. 9 Regressed curved surface of peak indentation depth correlated to UCS of rock material and uniaxial confining stress: (a) Three-dimensional view of curved surface; (b) View of curved surface from *X*-axis

and uniaxial confining stress were obtained from regression analysis. The expressions are given in Eqs. (9) and (10), and the illustrations are shown in Figs. 11 and 12, respectively.

$$W_c = 0.08793 \times (3.564 \times 10^{-4} \sigma_c^{2.3} \sigma_y^3 \, e^{-0.3526\sigma_y^{0.7}} + 1) \quad (9)$$

$$W_c = 0.4152 \times (2.153 \times 10^{-4} \sigma_c^{1.6} \sigma_t^{1.6} \sigma_y^3 \, e^{-0.5907\sigma_y^{0.6}} + 1) \quad (10)$$

3.2.4 Specific energy

Similar to the three-dimensional regression analyses mentioned above, the curved surfaces of

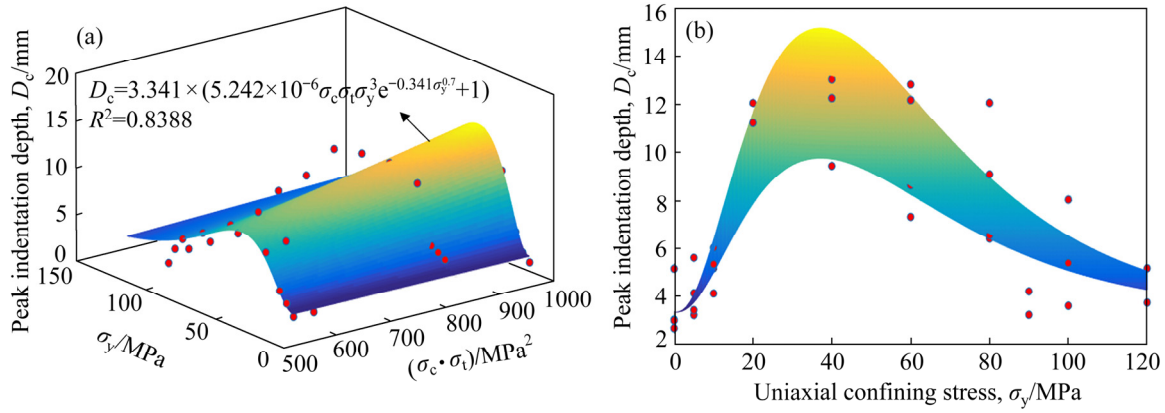

Fig. 10 Regressed curved surface of peak indentation depth correlated with uniaxial confining stress and product of UCS and tensile strength: (a) Three-dimensional view of regressed curved surface; (b) View of regressed curved surface from *X*-axis

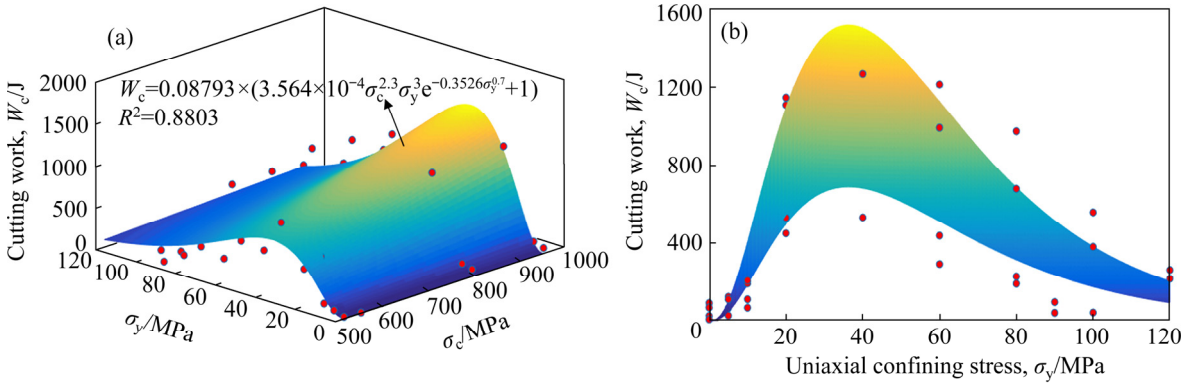

Fig. 11 Regressed curved surface of cutting work correlated to UCS of rock material and uniaxial confining stress: (a) Three-dimensional view of curved surface; (b) View of curved surface from *X*-axis

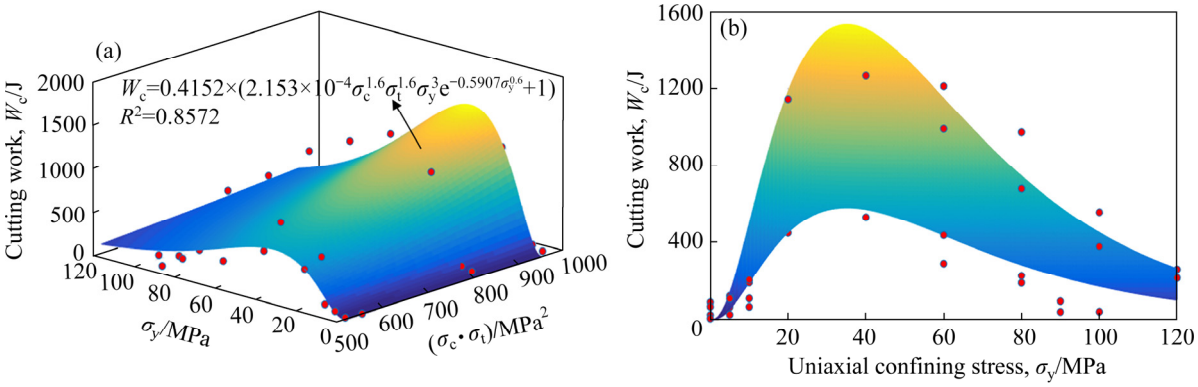

Fig. 12 Regressed curve surface of cutting work correlated to uniaxial confining stress applied to rock specimen and product of UCS and tensile strength of rock material: (a) Three-dimensional view of regressed curve surface; (b) View of regressed curve surface from *X*-axis

specific energy are expressed in Eqs. (11) and (12). The illustrations are shown in Figs. 13 and 14.

$$E_c = 0.9365 \times (1.062 \times 10^{-14} \sigma_c^{2.7} \sigma_y^9 \, e^{-0.09598\sigma_y^{1.1}} + 1) \quad (11)$$

$$E_c = 55.67 \times (1.041 \times 10^{-9} \sigma_c^{1.6} \sigma_t^{1.6} \sigma_y^5 \, e^{-0.09625\sigma_y} + 1) \quad (12)$$

3.2.5 Evaluation of models

Similar to the evaluation of two-dimensional regression model, RMSE and R^2 of three-dimensional model were obtained, as given in Table 5.

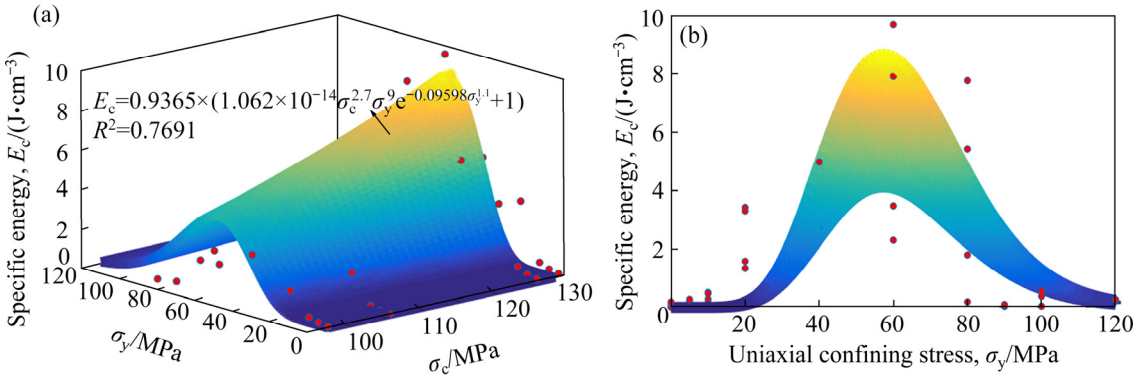

Fig. 13 Regressed curved surface of specific energy correlated to UCS of rock material and uniaxial confining stress: (a) Three-dimensional view of curved surface; (b) View of curved surface from *X*-axis

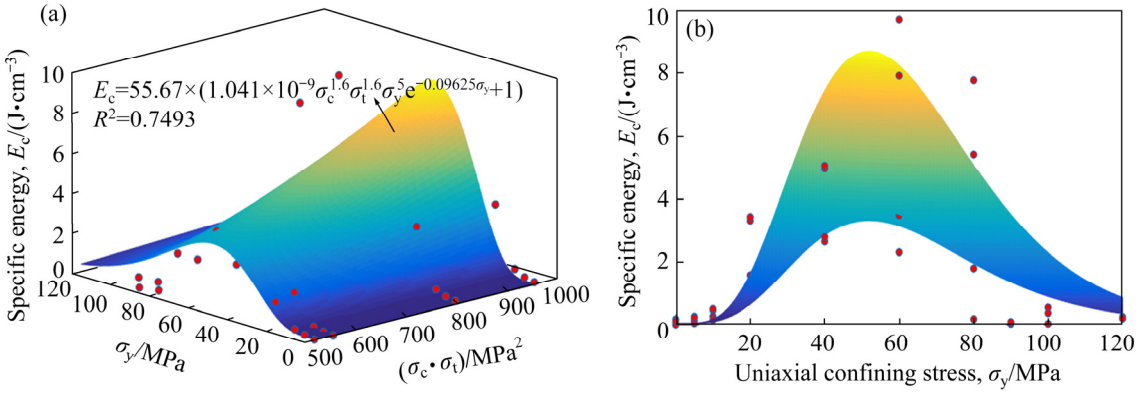

Fig. 14 Regressed curved surface of specific energy correlated to uniaxial confining stress applied to rock specimen and product of UCS and tensile strength of rock material: (a) Three-dimensional view of regressed curved surface; (b) View of regressed curved surface from *X*-axis

Table 5 RMSE and R^2 values of three-dimensional regression models

Regression type	Peak indentation force		Peak indentation depth		Cutting work		Specific energy	
	RMSE/kN	R^2	RMSE/mm	R^2	RMSE/J	R^2	RMSE/(10^{-3}J·cm^{-3})	R^2
UCS of rock material as *X*-axis	23.95	0.8473	1.19	0.8725	144.88	0.8803	1231.37	0.7691
Product of UCS and tensile strength of rock material as *X*-axis	26.96	0.8065	1.34	0.8388	158.27	0.8572	1281.72	0.7493

4 Prediction of rock cuttability using SVM and GRNN

The artificial intelligence technology has also been applied to the experiment. We adopt the support vector machine (SVM) and generalized neural network (GRNN) to predict the peak indentation force, peak indentation depth, cutting work and specific energy of rock breakage. The input parameters are composed of three parts, namely UCS of rock material, tensile strength of rock material and uniaxial confining stress.

4.1 Prediction of rock cuttability using SVM

4.1.1 SVM method and establishment

SVM is a typical machine learning method based on statistical theory [28]. The general structure diagram of SVM is shown in Fig. 15. In this work, SVM was used to predict and analyze the rock cuttability reflected by peak indentation force, peak indentation depth, cutting work and specific

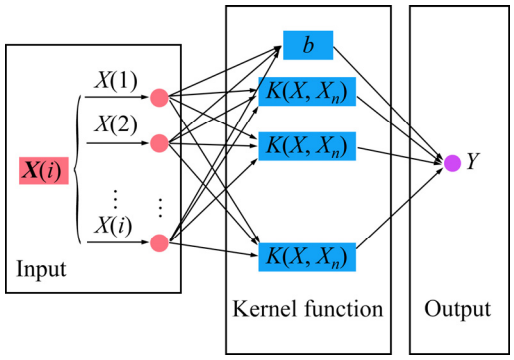

Fig. 15 General structure of SVM (***X***(*i*) is input support vector, $K(X, X_n)$ is kernel function, b is bias, and Y is output)

energy of conical pick for rock breakage.

4.1.2 Peak indentation force

In order to make the prediction results more universal and effective, the uniaxial confining stresses of 60, 40, 20 and 10 MPa were selected from granite, marble, red sandstone and phosphate rock as the test set, and the remaining 31 sets of data were taken as the training set. Normalization processing was adopted, and data were mapped to interval [0,1] with "mapminmax" function.

In order to verify the prediction accuracy of the established model, 31 groups of predicted results were compared with the experimental data by using the root-mean-squared error (RMSE) and determination coefficient (R^2). The illustrations of predicted and experimental results are shown in Fig. 16(a), and the corresponding RMSE and R^2 values are listed in Table 6.

By calculation using the trained SVM model, the predicted values of peak indentation forces were 153.7094, 203.3377, 99.2792 and 50.7648 kN, respectively. Compared with original experimental data, the prediction accuracies were 94.70%, 93.32%, 95.81% and 42.98%, respectively. The comparisons between predicted and experimental values for four groups of test data are shown in Fig. 17(a) and listed in Table 7.

Table 6 RMSE and R^2 values of SVM prediction models

Index	Peak indentation force/kN	Peak indentation depth/mm	Cutting work/J	Specific energy/(10^{-3}J·cm^{-3})
RMSE	16.4127	0.8919	16.1475	6.6888
R^2	0.7529	0.8275	0.9919	0.9990

Table 7 Comparisons between predicted results and experimental results for four groups of test data using SVM prediction

Cutting performance	Tested value	Predicted value	Accuracy/%
Peak indentation force, F_c/kN	162.33	153.7094	94.70
	217.90	203.3377	93.32
	103.62	99.2792	95.81
	32.33	50.7648	42.98
Peak indentation depth, D_c/mm	12.19	13.6944	87.66
	13.04	11.3134	86.76
	8.64	9.6448	88.37
	4.12	4.3564	94.26
Cutting work, W_c/J	989.40	989.6682	99.97
	1420.71	1421.0098	99.98
	447.64	447.4315	99.95
	66.60	77.3540	83.85
Specific energy, E_c/(10^{-3}J·cm^{-3})	7915.20	7914.1198	99.99
	4972.56	4972.9859	99.99
	1342.93	1343.4571	99.96
	166.50	162.2709	97.46

4.1.3 Peak indentation depth

The comparison results of predicted results and experimental data for 31 groups of training data are shown in Fig. 16(b), and the corresponding RMSE and R^2 values are listed in Table 6. By predication of the trained SVM model, the predicted values of peak indentation depth were 13.6944, 11.3134, 9.6448 and 4.3564 mm, respectively. Compared with original experimental data, the prediction accuracies were 87.66%, 86.76%, 88.37% and 94.26%, respectively. The comparisons between predicted and experimental values for four groups of test data are shown in Fig. 17(b) and listed in Table 7.

4.1.4 Cutting work

The comparison results of predicted results and experimental data for 31 groups of training data are shown in Fig. 16(c), and the corresponding RMSE and R^2 values are listed in Table 6. By using the trained SVM model, the predicted values of cutting work were 989.6682, 1421.0098, 447.4315 and 77.3540 J, respectively. Compared with the original experimental data, the prediction accuracies were 99.97%, 99.98%, 99.95% and 83.85%, respectively. The comparisons between predicted

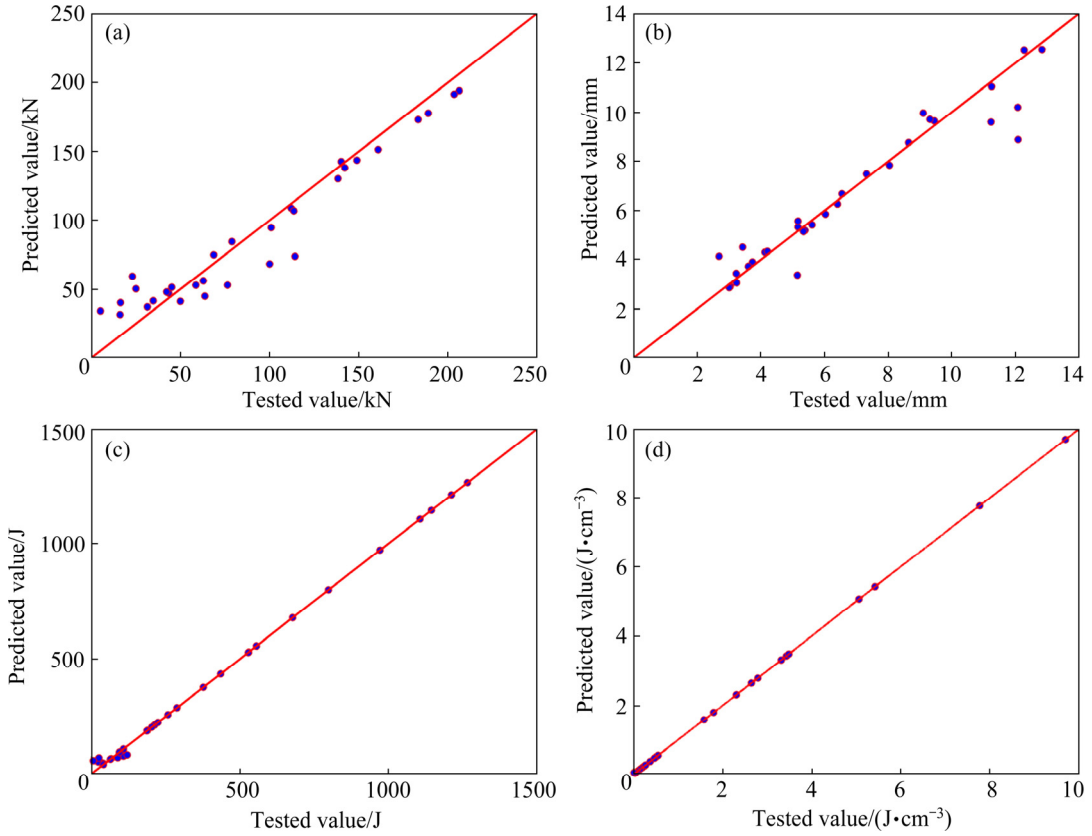

Fig. 16 Comparisons of predicted and experimental results for 31 groups of training data in SVM model: (a) Peak indentation force; (b) Peak indentation depth; (c) Cutting work; (d) Specific energy

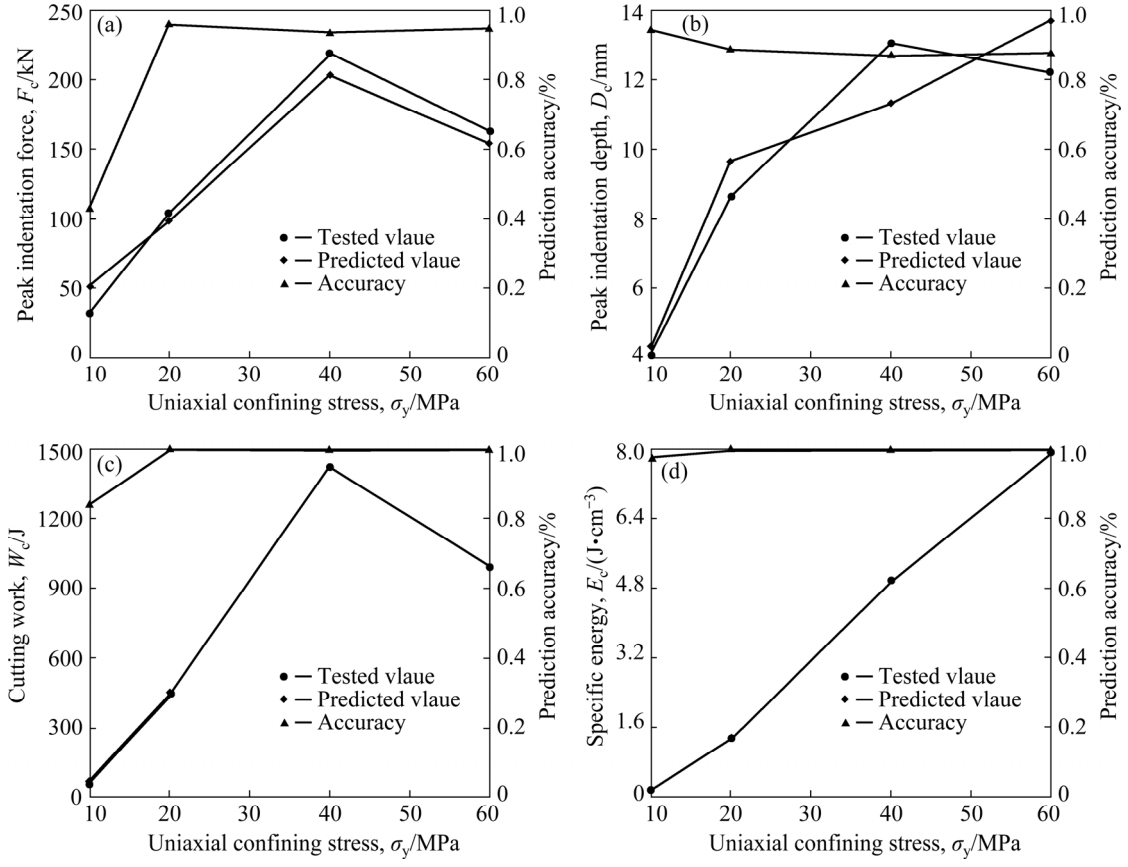

Fig. 17 Comparisons between predicted results using SVM and experimental results for four groups of test data

and experimental values for four groups of test data are shown in Fig. 17(c) and listed in Table 7.

4.1.5 Specific energy

The compared results of predicted results and experimental data for 31 groups of training data are shown in Fig. 16(d), and the corresponding RMSE and R^2 values are listed in Table 6. By using the trained SVM model, the predicted values of specific energy were 7914.1198, 4972.9859, 1343.4571 and 162.2709 J/cm^3, respectively. Compared with the original experimental data, the prediction accuracies were 99.99%, 99.99%, 99.96% and 97.46%, respectively. The comparisons between predicted and experimental values for four groups of test data are shown in Fig. 17(d) and listed in Table 7.

4.2 Prediction using GRNN

4.2.1 GRNN method and establishment

Generalized regression neural network (GRNN) is a kind of radial basis neural network [29]. The general GRNN model is shown in Fig. 18. The selections of training and test set of GRNN model were similar to the SVM model.

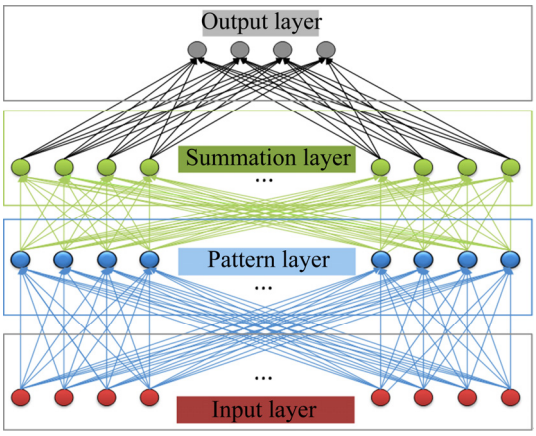

Fig. 18 General structure of GRNN model

4.2.2 Peak indentation force

After training, 31 groups of predicted results were compared with the experimental data. The illustration of predicted and experimental results is shown in Fig. 19(a), and the corresponding RMSE and R^2 values are listed in Table 8. By using the trained GRNN model, the predicted values of peak indentation force under the uniaxial confining stresses of 60 (granite), 40 (marble), 20 (red sandstone) and 10 MPa (phosphate rock) were 177.6150, 185.8675, 105.6953 and 36.2473 kN, respectively, and the corresponding prediction accuracies were 90.58%, 85.30%, 98.00% and 87.88%, respectively. The comparisons between the predicted and experimental values for four groups of test data are shown in Fig. 20(a) and listed in Table 9.

4.2.3 Peak indentation depth

The comparison results of predicted results and experimental data for 31 groups of training data are shown in Fig. 19(b), and the corresponding RMSE and R^2 values are listed in Table 8. The predicted values of peak indentation depth corresponding to four groups of test data were 10.6850, 12.4460, 9.0069 and 4.47 mm, respectively. Compared with the original experimental data, the prediction accuracies were 87.65%, 95.44%, 95.75% and 91.50%, respectively. The comparisons between predicted and experimental values for four groups of test data are shown in Fig. 20(b) and listed in Table 9.

4.2.4 Cutting work

The comparison results of predicted results and experimental data for 31 groups of training data are shown in Fig. 19(c), and the corresponding RMSE and R^2 values are listed in Table 8. The predicted values of cutting works corresponding to four groups of tests data were 971.6250, 1158.8800, 528.3222 and 68.2585 J, respectively. Compared with the original experimental data, the prediction accuracies were 98.20%, 81.57%, 81.98% and 97.51%, respectively. The comparisons between predicted and experimental values for four groups of test data are shown in Fig. 20(c) and listed in Table 9.

4.2.5 Specific energy

The comparison results of predicted results after the training of GRNN model and experimental data for 31 groups of training data are shown in Fig. 19(d), and the corresponding RMSE and R^2 values are listed in Table 8. The predicted values of specific energy corresponding to four groups of test data were 6502.8115, 4014.3037, 1029.2626, 109.3745 J/cm^3, respectively. Compared with the original experimental data, the prediction accuracies were 82.16%, 80.73%, 76.64%, 65.69%, respectively. The comparisons between predicted and experimental values for four groups of test data are shown in Fig. 20(d) and listed in Table 9.

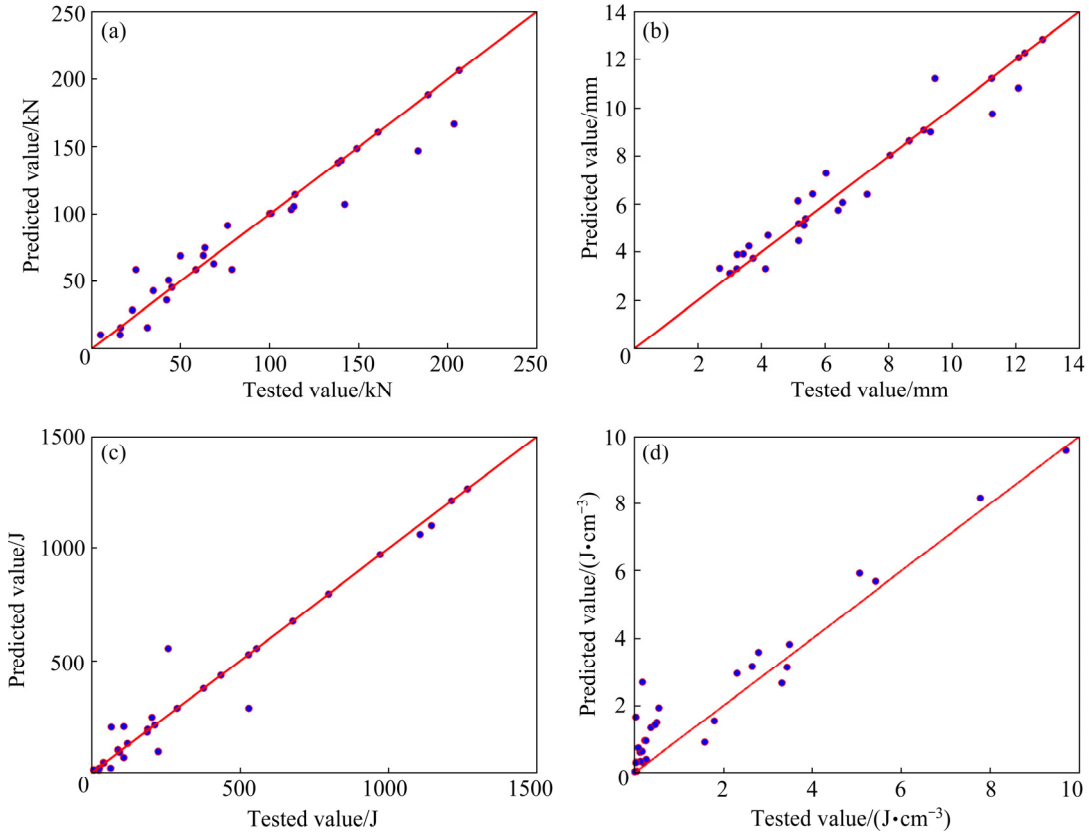

Fig. 19 Comparisons of predicted and experimental results for 31 groups of training data in GRNN model: (a) Peak indentation force; (b) Peak indentation depth; (c) Cutting work; (d) Specific energy

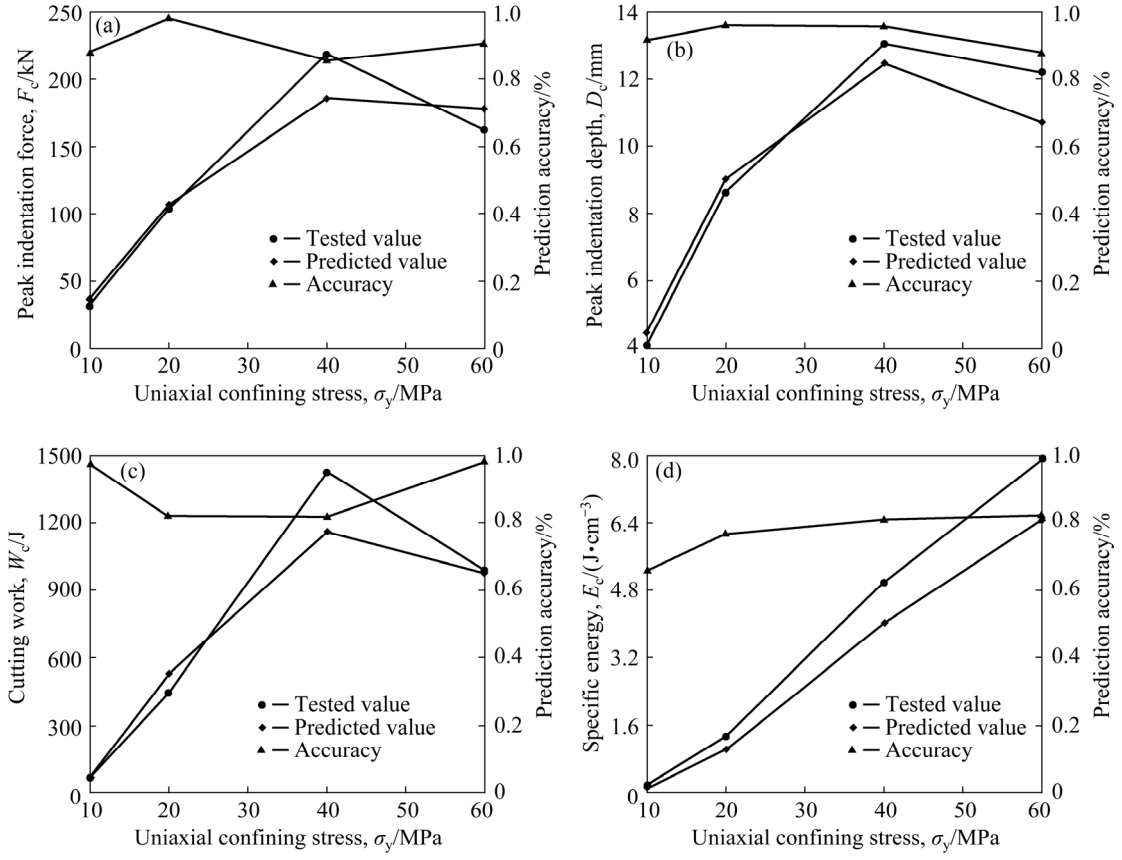

Fig. 20 Comparisons between predicted results using GRNN and experimental results for four groups of test data

Table 8 RMSE and R^2 values of GRNN prediction models

Index	Peak indentation force/kN	Peak indentation depth/mm	Cutting work/J	Specific Energy/ (10^{-3}J·cm^{-3})
RMSE	14.8097	0.6878	80.6582	789.3227
R^2	0.8210	0.9161	0.9681	0.9708

Table 9 Comparisons between predicted results and experimental results for four groups of test data using GRNN prediction

Cutting performance	Tested value	Predicted value	Accuracy/ %
Peak indentation force, F_c/kN	162.33	177.6150	90.58
	217.90	185.8675	85.30
	103.62	105.6953	98.00
	32.33	36.2473	87.88
Peak indentation depth, D_c/mm	12.19	10.6850	87.65
	13.04	12.4460	95.44
	8.64	9.0069	95.75
	4.12	4.4700	91.50
Cutting work, W_c/J	989.40	971.625	98.20
	1420.71	1158.880	81.57
	447.64	528.3222	81.98
	66.60	68.2585	97.51
Specific energy, E_c/(10^{-3}J·cm^{-3})	7915.20	6502.8115	82.16
	4972.56	4014.3037	80.73
	1342.93	1029.2626	76.64
	166.50	109.3745	65.69

5 Discussion

5.1 Influence of uniaxial confining stress

According to the regression analyses of peak indentation force, peak indentation depth, cutting work and specific energy of conical pick for rock breakage, uniaxial confining stress had a nonlinear influence on rock cuttability. Peak indentation force, peak indentation depth, cutting work and specific energy presented nonlinear variation with first increasing followed by decreasing as uniaxial confining stress was increased, which indicated that the rock cuttability first decreased and then increased as uniaxial confining stress was increased. In addition, the failure patterns of rock specimens were changed from complete splitting to partial splitting, and then to rockburst as uniaxial confining stress was increased. The experimental and regressive results showed that there were three zones reflecting the influence of uniaxial confining stress on rock cuttability. In Zone 1, the increasing of uniaxial confining stress impeded the rock cutting. In Zone 2, the increasing of uniaxial confining stress improved the rock cutting. The demarcation point between Zone 1 and Zone 2 was at the uniaxial confining stress near 30%−40% of UCS of rock material in terms of peak indentation force, peak indentation depth and cutting work and near 40%−55% of UCS of rock material in terms of specific energy. In Zone 3, the increasing of uniaxial confining stress continued to improving the rock cutting, and only very low specific energy was required for rock breakage promoted by high uniaxial confining stress. However, the rock compressed by high uniaxial confining stress produced rockburst induced by point-load disturbance of rock cutting. The demarcation point between Zone 2 and Zone 3 was at the uniaxial confining stress near 80% of UCS of rock material in terms of peak indentation force, peak indentation depth, cutting work and specific energy.

5.2 Influence of rock strength

It can be seen from the three-dimensional regression models that the peak indentation force, peak indentation depth, cutting work and specific energy of conical pick required for rock breakage presented a positive correlation to the UCS and tensile strength of rock material, which indicated that the rock strength had a negative influence on rock cuttability. Therefore, the high cutting parameters such as peak indentation force, peak indentation depth, cutting work and specific energy should be required for breakage of hard rock. The demarcation points for distinguishing the stress-impediment zone (Zone 1) and the stress-improvement zone (Zone 2) of rock cuttabilities were correlated to the UCS of rock material, which were near 30%−40% of UCS of rock material in terms of peak indentation force, peak indentation depth and cutting work and near 40%−55% of UCS of rock material in terms of specific energy. The demarcation points for distinguishing the stress-improvement zone (Zone 2) and the cutting-triggered rockburst zone (Zone 3) of rock cuttabilities were also correlated to the UCS of rock

material, which were near 80% of UCS of rock material in terms of peak indentation force, peak indentation depth, cutting work and specific energy.

5.3 Field mining application

It can be calculated that the prediction effect of SVM is better than GRNN, according to the compared analyses between predicted and experimental results for 31 groups of training data and the verified comparisons between predicted and experimental results for four groups of test data. In addition, the experimental results, regressive analyses and AI-based predictions showed that the rock cuttability, negatively reflected by peak indentation force, peak indentation depth, cutting work and specific energy of conical pick for rock breakage in rock indentation test, first decreased and then increased with the increase in uniaxial confining stress, and the rock cuttability was negatively correlated to UCS and tensile strength of rock material. Meanwhile, the risk of rockburst increased obviously under the high uniaxial confining stress, which indicated that the rock intensively compressed by high uniaxial stress was prone to violent failure with rapid ejection of fragments triggered by rock indentation, although the rock cuttability was improved by high stress. Therefore, the rocks under free stress and low confining stress have the best rock cuttability and cutting safety. In order to further verify the models for predicting rock cuttability and confirm the feasibility of rock cutting by conical pick, a field mining stope was prepared in Kaiyang Phosphate Mine, Guizhou Province, China, to perform rock cutting. The preparation and cutting entryways were excavated to form a pillar. The residual stress in rock around pillar was uniaxial confining stress, the variation range of which was from stress-free condition to 14.5 MPa. The maximum cutting parameters of peak indentation force, peak indentation depth, cutting work and specific energy were predicted by regressed and SVM-based models, and the results are listed in Table 10. Finally, a roadheader with many conical picks mounted was used to perform rock cutting on ore-rock pillar, and the cutting parameters were designed according to the predicted results. The mean cutting efficiency reached 107.7 t/h. The roadheader met the requirement of mechanized mining in hard rock around the pillar, and the prediction models were suitable for guiding the rock cutting by conical pick.

Table 10 Maximum rock cutting parameters predicted by regressed model and SVM for phosphate rock under maximum residual uniaxial confining stress of 14.5 MPa

Prediction method	Peak indentation force, F_c/kN	Peak indentation depth, D_c/mm	Cutting work, W_c/J	Specific energy, E_c/(10^{-3}J·cm^{-3})
Regressed model	69.02	6.58	356.74	282.97
SVM	60.14	5.91	350.90	951.32

6 Conclusions

(1) The regression models can reflect the relationships of peak indentation force, peak indentation depth, cutting work and specific energy with the uniaxial confining stress applied to rock and the UCS and tensile strength of rock. The prediction accuracy from SVM was better than that from GRNN. Therefore, the regression and SVM models are satisfactory for predicting the rock cuttability reflected by peak indentation force, peak indentation depth, cutting work and specific energy of conical pick for rock breakage in the rock indentation test.

(2) The experimental results, regressive analyses and AI-based predictions indicated that the peak indentation force, peak indentation depth, cutting work and specific energy of conical pick for rock breakage increased and then decreased with the increase in uniaxial confining stress, and these indices were positively correlated to UCS and tensile strength of rock materials. The rocks under free stress and low uniaxial confining stress can be cut efficiently and safely, while the rockburst occurred in the rock under high uniaxial confining stress, although the rock cuttability can be improved by high stress. Therefore, the rocks under free stress and low confining stress had the best rock cuttability and cutting safety.

(3) The regressed and SVM-based models were used to predict the cutting parameters of roadheader in the mining filed. The axial boom roadheader with many conical picks mounted were used to perform rock cutting around pillar. The cutting efficiencies reached 107.7 t/h. The roadheader can satisfy the requirement of

mechanized mining in hard rock, and the established prediction models can be suitable for guiding the rock cutting by conical pick.

Acknowledgments

The authors are grateful for the financial supports from the National Natural Science Foundation of China (Nos. 51904333, 51774326).

References

[1] BILGIN N, COPUR H, BALCI C. Mechanical excavation in mining and civil industries [M]. Boca Raton: CRC Press, Taylor & Francis Group, 2013.

[2] WANG Shao-feng, SUN Li-cheng, HUANG Lin-qi, LI Xi-bing, SHI Ying, YAO Jin-rui, DU Shao-lun. Non-explosive mining and waste utilization for achieving green mining in underground hard rock mine in China [J]. Transactions of Nonferrous Metals Society of China, 2019, 29(9): 1914−1928.

[3] DU Kun, LI Xi-bing, TAO Ming, WANG Shao-feng. Experimental study on acoustic emission (AE) characteristics and crack classification during rock fracture in several basic lab tests [J]. International Journal of Rock Mechanics and Mining Sciences, 2020, 133: 104411.

[4] LI Xi-bing, WANG Shao-feng, WANG Shan-yong. Experimental investigation of the influence of confining stress on hard rock fragmentation using a conical pick [J]. Rock Mechanics and Rock Engineering, 2018, 51: 255−277.

[5] WANG Shao-feng, HUANG Lin-qi, LI Xi-bing. Analysis of rockburst triggered by hard rock fragmentation using a conical pick under high uniaxial stress [J]. Tunnelling and Underground Space Technology, 2020, 96: 103195.

[6] WANG Shao-feng, LI Xi-bing, YAO Jin-rui, GONG Feng-qiang, LI Xiang, DU Kun, TAO Ming, HUANG Lin-qi, DU Shao-lun. Experimental investigation of rock breakage by a conical pick and its application to non-explosive mechanized mining in deep hard rock [J]. International Journal of Rock Mechanics and Mining Sciences, 2019, 122: 104063.

[7] CAO Wen-zhuo, SHI Ji-quan, SI Guang-yao, DURUCAN S, KORRE A. Numerical modelling of microseismicity associated with long wall coal mining [J]. International Journal of Coal Geology, 2018, 193: 30−45.

[8] LI X B, CHEN Z H, WENG L, LI C J. Unloading responses of pre-flawed rock specimens under different unloading rates [J]. Transactions of Nonferrous Metals Society of China, 2019, 29(7): 1516−1526.

[9] QIU J D, LI X B, LI D Y, ZHAO Y Z, HU C W, LIANG L S. Physical model test on the deformation behavior of an underground tunnel under blasting disturbance [J]. Rock Mechanics and Rock Engineering, 2020, Doi: 10.1007/s00603-020-02249-2.

[10] CAI X, ZHOU Z L, ZANG H Z, SONG Z Y. Water saturation effects on dynamic behavior and microstructure damage of sandstone: Phenomena and mechanisms [J]. Engineering Geology, 2020, 276: 105760.

[11] DANG W G, KONIETZKY H, FRUHWIRT T, HERBST M. Cyclic frictional responses of planar joints under cyclic normal load conditions: Laboratory tests and numerical simulations [J]. Rock Mechanics and Rock Engineering, 2020, 53: 337−364.

[12] LIU Zhi-xiang, LUO Tian, LI Xiang, LI Xi-bing, HUAI Zhen, WANG Shao-feng. Construction of reasonable pillar group for undersea mining in metal mine [J]. Transactions of Nonferrous Metals Society of China, 2018, 28(4): 757−765.

[13] BILGIN N, DEMIRCIN M A, COPUR H, BALCI C, TUNCDEMIR H, AKCIN N. Dominant rock properties affecting the performance of conical cutters and the comparison of some experimental and theoretical results [J]. International Journal of Rock Mechanics and Mining Sciences, 2006, 43: 139−156.

[14] BALCI C, BILGIN N. Correlative study of linear small and full-scale rock cutting tests to select mechanized excavation machines [J]. International Journal of Rock Mechanics and Mining Sciences, 2007, 44: 468−476.

[15] COPUR H, BILGIN N, BALCI C, TUMAC D, AVUNDUK E. Effects of different cutting patterns and experimental conditions on the performance of a conical drag tool [J]. Rock Mechanics and Rock Engineering, 2017, 50(6): 1585−1609.

[16] EVANS I. A theory of the cutting force for point-attack picks [J]. International Journal of Mining Engineering, 1984, 2(1): 63−71.

[17] GOKTAN R M, GUNES N. A semi-empirical approach to cutting force prediction for point-attack picks [J]. Journal of the Southern African Institute of Mining and Metallurgy, 2005, 105(4): 257−263.

[18] ROJEK J, ONATE E, LABRA C, KARGL H. Discrete element simulation of rock cutting [J]. International Journal of Rock Mechanics and Mining Sciences, 2011, 48: 996−1010.

[19] ZHAO Gao-feng, LIAN Ji-jian, RUSSELL A R, ZHAO Jian. Three-dimensional DDA and DLSM coupled approach for rock cutting and rock penetration [J]. International Journal of Geomechanics, 2017, 17(5): E4016015.

[20] GRIMA M A, BRUINES P A, VERHOEF P N W. Modeling tunnel boring machine performance by neuro-fuzzy methods [J]. Tunnelling Underground Space Technology, 2000, 15: 259−269.

[21] BENARDOS A G, KALIAMPAKOS D C. Modelling TBM performance with artificial neural networks [J]. Tunnelling Underground Space Technology, 2004, 19: 597−605.

[22] YAGIZ S, GOKCEOGLU C, SEZER E, IPLIKCI S. Application of two nonlinear prediction tools to the estimation of tunnel boring machine performance [J]. Engineering Applications of Artificial Intelligence, 22: 808−814.

[23] YAGIZ S, KARAHAN H. Prediction of hard rock TBM penetration rate using particle swarm optimization [J]. International Journal of Rock Mechanics and Mining Sciences, 2011, 48: 427−433.

[24] GHASEMI E, YAGIZ S, ATAEI M. Predicting penetration rate of hard rock tunnel boring machine using fuzzy logic [J]. Bulletin of Engineering Geology and the Environment, 2014, 73: 23−35.

[25] MAHDEVARI S, SHAHRIAR K, YAGIZ S, SHIRAZI M A. A support vector regression model for predicting tunnel boring machine penetration rates [J]. International Journal of Rock Mechanics and Mining Sciences, 2014, 72: 214−229.
[26] ARMAGHANI D J, MOHAMAD E T, NARAYANASAMY M S, NARITA N, YAGIZ S. Development of hybrid intelligent models for predicting TBM penetration rate in hard rock condition [J]. Tunnelling Underground Space Technology, 2017, 63: 29−43.
[27] WANG Shao-feng, LI Xi-bing, DU Kun, WANG Shan-yong, TAO Ming. Experimental study of the triaxial strength properties of hollow cylindrical granite specimens under coupled external and internal confining stresses [J]. Rock Mechanics and Rock Engineering, 2018, 51: 2015−203.
[28] CRISTIANINI N, SHAWE-TAYLOR J. An introduction to support vector machines and other kernel-based learning methods [M]. Cambridge: Cambridge University Press, 2000.
[29] SPECHT D F. A general regression neural network [J]. IEEE Transactions on Neural Networks, 1991, 2(6): 568−576.

基于镐形截齿侵入破岩试验的岩石可切割性分析与预测

王少锋[1]，唐 宇[1]，李夕兵[1]，杜 坤[1,2]

1. 中南大学 资源与安全工程学院，长沙 410083；
2. 中南大学 高等研究中心，长沙 410083

摘 要：为了研究围压条件和岩石强度参数对岩石可切割性的影响，开展一系列镐形截齿侵入破岩试验。利用回归分析、支持向量机(SVM)和广义回归神经网络(GRNN)分析岩石可切割性与施加在岩石上的单轴围压和岩石强度参数(单轴抗压强度和抗拉强度)之间的关系。得到的回归模型和 SVM 模型可以准确反映岩石可切割性的变化规律。分析结果表明，随着单轴围压的增加，岩石的可切割性先降低后增加，岩石的可切割性与岩石抗压强度和抗拉强度呈负相关。根据预测模型计算得到镐型截齿切割坚硬磷矿石的最佳应力条件和切割参数，从而使基于多截齿旋转切割的纵轴悬臂式掘进机成功应用于坚硬磷矿石的开采。

关键词：岩石可切割性；侵入破岩；预测模型；回归分析；支持向量机；神经网络

(Edited by Bing YANG)